



# Building an Acceleration Ladder with Tidal Streams and Pulsar Timing

Peter Craig<sup>1</sup>, Sukanya Chakrabarti<sup>2</sup>, Robyn E. Sanderson<sup>3</sup>, and Farnik Nikakhtar<sup>4</sup>

<sup>1</sup> Department of Physics and Astronomy, Rochester Institute of Technology, Rochester, NY, 14623, USA; [pac4607@rit.edu](mailto:pac4607@rit.edu)

<sup>2</sup> Department of Physics and Astronomy, University of Alabama, Huntsville, Huntsville, AL, 35899, USA

<sup>3</sup> Department of Physics and Astronomy, University of Pennsylvania, Philadelphia, PA, 19104, USA

<sup>4</sup> Department of Physics, Yale University, New Haven, CT, 06520, USA

Received 2022 November 1; revised 2023 January 30; accepted 2023 February 8; published 2023 March 13

## Abstract

We analyse stellar streams in action-angle coordinates combined with recent local direct acceleration measurements to provide joint constraints on the potential of our galaxy. Our stream analysis uses the Kullback–Leibler divergence with a likelihood analysis based on the two-point correlation function. We provide joint constraints from pulsar accelerations and stellar streams for local and global parameters that describe the potential of the Milky Way (MW). Our goal is to build an “acceleration ladder,” where direct acceleration measurements that are currently limited in dynamic range are combined with indirect techniques that can access a much larger volume of the MW. To constrain the MW potential with stellar streams, we consider the Palomar 5, Orphan, Nyx, Helmi, and GD1 streams. Of the potential models that we have considered here, the preferred potential for the streams is a two-component Staekel potential. We also compare the vertical accelerations from stellar streams and pulsar timing, defining the function  $f(z) = \alpha_{1\text{pulsar}}z - \frac{\partial\Phi}{\partial z}$ , where  $\Phi$  is the MW potential determined from stellar streams and  $\alpha_{1\text{pulsar}}z$  is the vertical acceleration determined from pulsar timing observations. Our analysis indicates that the Oort limit determined from streams is consistently (regardless of the choice of potential) lower than that determined from pulsar timing observations. The calibration we have derived here may be used to correct the estimate of the acceleration from stellar streams.

*Unified Astronomy Thesaurus concepts:* Milky Way mass (1058); Milky Way dynamics (1051); Milky Way dark matter halo (1049)

## 1. Introduction

The signatures of tidal interactions between galaxies carry valuable information about the Galactic potential and the interaction itself, encoded in the orbital properties of stream member stars (Johnston et al. 1999; Newberg et al. 2002; Price-Whelan & Johnston 2013; Sanderson et al. 2015), or in disturbances in the stream gas (Levine et al. 2006; Weinberg & Blitz 2006; Chakrabarti & Blitz 2009, 2011; Chakrabarti et al. 2011; Chakrabarti 2013; Craig et al. 2021). Streams (both stellar and gaseous) have been used to constrain the Milky Way (MW) halo potential out to large distances (Koposov et al. 2010; Malhan & Ibata 2019; Reino et al. 2021; Vasiliev et al. 2021), and have also been used to constrain dark matter substructure (Carlberg et al. 2012; Carlberg & Grillmair 2013; Sanders et al. 2016; Erkal et al. 2017; Bonaca et al. 2019, 2020; Banik & Bovy 2019).

Recently, extreme-precision time-series observations to measure Galactic accelerations and the Galactic potential directly have become feasible. Chakrabarti et al. (2021a) analysed compiled pulsar timing observations to measure the Galactic acceleration and derive fundamental Galactic parameters, including the Oort limit (the midplane density), the local dark matter density, and the shape of the Galactic potential. In the near future, we can expect direct acceleration measurements from extreme-precision radial velocity observations (Chakrabarti et al. 2020) and from eclipse timing (Chakrabarti et al. 2021b). Although direct acceleration

measurements have provided local constraints on the potential (Chakrabarti et al. 2021a), they do not yet provide constraints for the MW’s mass or other global parameters for which we require information over a large volume. While stellar streams provide indirect constraints, they add valuable information about the shape and extent of the MW potential at larger distances. Here, we explore the idea that combining complementary information from local acceleration measurements and tidal streams can be used to build an “acceleration ladder” to derive constraints on the Galactic potential.

Several methods have been used to extract information about the Galactic potential from tidal streams. One is to fit an orbit to a stream based on the observed positions and velocities along the stream, as done in Newberg et al. (2010) and Koposov et al. (2010). Agreement between the stream orbits and the data is potential-dependent, allowing a fitting procedure to be used to estimate the parameters of the MW potential. There are known biases in this methodology that result from differences between the orbits of stream stars and the progenitor (Sanders & Binney 2013). An alternative method is to back-integrate the orbits of stream member stars in the MW potential (Price-Whelan et al. 2014). If these orbits are calculated using an accurate MW potential, then the member stars should become bound to the progenitor at some point in their orbital history. Another common technique is the forward modeling method, such as the one described in Bonaca et al. (2014), which has several related variations (Varghese et al. 2011; Sanders 2014; Fardal et al. 2015). This method uses a Markov Chain Monte Carlo algorithm that compares simulated streams to observed streams in 6D phase space.

We focus here on stellar streams rather than gaseous streams to take advantage of the vast infrastructure that has been



Original content from this work may be used under the terms of the [Creative Commons Attribution 4.0 licence](https://creativecommons.org/licenses/by/4.0/). Any further distribution of this work must maintain attribution to the author(s) and the title of the work, journal citation and DOI.

developed for the collisionless components of galaxies (Binney & Tremaine 2008), and the better distance estimates that are available for stars in stellar streams relative to the kinematic distance estimates that are typically available for the gas (Levine et al. 2006). We employ the action space clustering method developed in Sanderson et al. (2015), and later applied in Reino et al. (2021). In the true potential, stream stars that were once part of a disrupted dwarf galaxy are expected to be on similar orbits, and thus have similar positions in action space. We apply this by searching for the potentials that lead to the strongest clustering in the actions of stream stars. Since actions are integrals over one period of the orbit, this method is similar to the “rewinder” algorithm of Price-Whelan & Johnston (2013). The analysis of stellar streams by Sanderson et al. (2017) employs a “consensus fit” whereby multiple streams provide information on various regions of the MW potential, allowing the potential model to be valid over larger parts of the galaxy; another advantage of this approach is that the consideration of multiple streams leads to a smaller bias than one stream alone (Bonaca et al. 2014), i.e., due to the disrupted dwarf galaxy being near pericenter, which can bias the results (Reino et al. 2022). It has been demonstrated based on Aquarius simulations that these methods are effective at recovering the present-day properties of the host galaxy potential (Sanderson et al. 2017). A limitation of these techniques is that they do not extend well to models of potentials that are not in equilibrium or are time-dependent, so these effects cannot be captured. Our goal is to recover the present-day properties of the MW potential, as this is what the direct accelerations probe, so this method works well for our purposes.

One of the challenges to using tidal streams for measuring the Galactic potential is obtaining 6D phase-space information for the member stars. High-quality positions and proper motions can typically be obtained from Gaia data (Gaia Collaboration et al. 2016, 2018), significantly expanding the sample of stars with available information (Bonaca et al. 2014). To get to full 6D information we also require distances and radial velocities. For some streams, missing measurements can be estimated by fitting the distances or radial velocities along a stream track, then interpolating based on the positions in the stream. The same method is used in Reino et al. (2021) for the streams considered here, and for Sagittarius in Vasiliev et al. (2021).

One of our goals is to use recent direct acceleration measurements from pulsar timing to calibrate indirect measurements for the potential of the MW. This would in effect serve to build an “acceleration ladder,” similar to the distance ladder that is based on the calibration of indirect distance measurements using the basic geometric measurements of distances obtained from parallax measurements. Direct acceleration measurements provide the first rung of the ladder, i.e., a “pivot point” for the Galactic potential, which can be used to calibrate stream-based potential measurements. In Reino et al. (2021), only models that matched the circular velocities at the solar circle to within the uncertainties were considered, where the measurements of the circular velocities were indirect, while our pulsar accelerations provide a direct measurement of the potential. The paper is organized as follows. We present our methodology in Section 2 and discuss our data selection in

Section 3. We present our main results in Section 4, and conclude in Section 5.

## 2. Methods

We use the Python package GALPY (Bovy 2015) to calculate the actions for our streams. They are calculated analytically for the isochrone potential (Binney & Tremaine 2008), and numerically in all other potentials considered. In spherically symmetric potentials, like the Hernquist potential, we use GALPY’S spherical approximation method, providing accurate and efficient action calculations. Staeckel potentials allow us to use Staeckel approximations, providing accurate actions requiring only a single numerical integral for each action (Bonaca et al. 2014). For all other potentials, we use the isochrone approximation method in GALPY. This method uses an auxiliary isochrone potential with integrated orbits of the stars in the desired potential to compute the actions. This requires orbit integration for each star, and is therefore relatively computationally intensive. However, this provides more accurate approximations to the actions in these potentials compared to other methods. In particular, the assumptions made for the other methods break down when the radial or vertical actions are of the same order as  $L_z$  (Bovy 2014).

For each potential model, we tested the accuracy of the action approximations by calculating the actions of all our stream members along their orbits for a variety of different points in the parameter space. We use a leapfrog algorithm to compute the orbit for at least one orbital period, and then calculate the actions at regular intervals along the orbit. The actions should remain constant, and we find that the action variations are consistently less than 1% in  $J_R$  and  $J_z$ . When we use data from multiple streams, we shift the actions in  $L_z$  for each individual stream such that there is limited overlap between streams. This will not impact the clustering in action space, but helps to avoid error modes with large masses and low scale lengths (Reino et al. 2021).

As we intend to build upon the results from direct acceleration measurements from pulsar timing, we consider the potentials used in Chakrabarti et al. (2021a). Specifically, we consider the  $\alpha_1$  potential and the  $\alpha\gamma$  potential. These are defined in Equations (1) and (2), respectively, where  $\alpha_1$  is the inverse square of the frequency of low-amplitude vertical oscillations,  $V_{\text{LSR}}$  is the local standard of rest velocity, and  $\gamma$  describes the shape of the potential. The  $\alpha_1$  potential provided the best fit to the pulsar accelerations, and the  $\alpha\gamma$  potential is the “cross-term” model discussed in Chakrabarti et al. (2021a). These models provide a good match to the measured pulsar accelerations, however they do not produce strong clustering in action space. This is expected because these models were designed to produce reasonable orbits for stars in the solar neighborhood with low eccentricities and inclinations, which are not generally satisfied by our stream members (Quillen et al. 2020).

$$\Phi(R, z) = V_{\text{LSR}}^2 \log(R/R_\odot) + \frac{1}{2}\alpha_1 z^2 \quad (1)$$

$$\Phi(R, z) = V_{\text{LSR}}^2 \log(R/R_\odot) + \log(R/R_\odot)\gamma z^2 + \frac{1}{2}\alpha_1 z^2. \quad (2)$$

## 2.1. KLD

We use the Kullback–Leibler divergence (KLD) to measure the amount of clustering in action space, as in Sanderson et al. (2015). The KLD compares two probability density functions (PDFs) to each other. We use it to measure the amount of action space clustering by comparing the action distribution with a uniform distribution over the maximum range for each action across all the data sets (potentials and streams). Larger KLD values indicate a larger difference between the distributions, implying that there is more clustering in action space. Equation (3) defines the KLD for a continuous random variable from  $p(x)$  to  $q(x)$ , where in our case  $p(x)$  will be the action distribution and  $q(x)$  will be our uniform distribution:

$$\text{KLD}(p: q) = \int p(x) \log\left(\frac{p(x)}{q(x)}\right) dx. \quad (3)$$

We use the kernel density estimator ENBID (Sharma & Steinmetz 2011) to estimate the PDF for the actions. We define the resulting distribution for a potential with parameter  $a$  as  $f_a(J)$ , and then we can calculate the KLD from Equation (4). This integral can be rewritten as in Reino et al. (2021) using a Monte Carlo approximation to sum across points drawn from the distribution. This is a natural choice in our case where we have a discrete set of actions corresponding to our member stars. The exact form of the calculation used corresponds to the wKLD1 given in Reino et al. (2021), which includes a weight term such that the streams contribute equally in joint fits and can be seen in Equation (5). In this equation,  $N_s$  is the number of streams in the sample,  $N_j$  is the number of stars in a stream, and  $u(J)$  is a uniform distribution of actions. Here  $p(J|\zeta, \omega)$  is the PDF of the actions  $J$  with potential parameters  $\zeta$  and phase space positions. This formulation is designed to give each stream equal weight in the KLD calculations.

$$D_{\text{KL}}^1 = \int f_a(J) \log\left(\frac{f_a(J)}{f_a^{\text{shuf}}(J)}\right) d^3J. \quad (4)$$

$$w\text{KLD1}(\zeta) = \sum_j \sum_i \frac{1}{N_s N_j} \log \frac{p(J|\zeta, \omega)}{u(J)} \bigg|_{J=J_j^{ij}} \quad (5)$$

For our data set, we use an optimization algorithm to find the maximum value of the KLD within reasonable bounds. For two parameter potentials, we apply a simple grid search across the parameter space. The same grid can be used for the error analysis technique described in Reino et al. (2021) and Sanderson et al. (2015), which measures the KLD between the best-fitting action distribution and the distributions in other potentials. For potentials with more than two parameters, we use a differential evolution optimizer implemented in SCIPY (Virtanen et al. 2020) to maximize the KLD.

## 2.2. Likelihoods and Error Analysis

We use the two-point correlation function to compute the likelihood from the action distributions in order to compare with the pulsar sample. We use the likelihoods from both methods and combine them to get a joint likelihood function. The likelihoods for the streams are calculated using the methods given in Yang et al. (2020). This approach is different from that used in Reino et al. (2021), chosen here because it enables the combination of our methods.

We can use the likelihoods to estimate the uncertainties by examining the relative likelihood (i.e., the likelihood divided

by the maximum likelihood value) for the parameters that we are interested in. A confidence region in parameter space can be defined by setting a threshold on the relative likelihoods corresponding to the desired confidence interval. We generally focus on the total mass and Oort limit for the various potentials, but also compute a surface across all parameters to measure their uncertainties. We considered using a Fisher matrix analysis to compute the uncertainties. However, this analysis underestimates the uncertainties for the streams. The likelihood surfaces can have multiple local maxima near the maximum likelihood, corresponding to the best fits of individual streams. Since the Fisher matrix analysis is based on the derivatives of the likelihood function, it is only sensitive to regions near the maximum likelihood, leading to an underestimation of the uncertainties.

The combined sample (i.e., for pulsars and streams) has a likelihood surface defined by the product of the two individual likelihoods, which gives us the relative likelihoods for the combined sample. In this way we can easily obtain the uncertainties for both the individual and combined samples using the same mechanism.

For all the potentials considered except for the  $\alpha_1$  potential, we examine the total masses and Oort limits for the models. In cases with more than two parameters we marginalize over the remaining parameters to produce a two-dimensional likelihood surface. We expect the streams to produce better constraints on the total mass, while the pulsars should provide stronger constraints on the Oort limit. Thus, we expect the combined sample to provide tighter constraints than either individual sample.

Note that we do not use a maximum likelihood analysis to find the best-fitting parameters, instead we maximize the KLD as described above. From our likelihood surfaces we have confirmed that the best-fitting KLD parameters closely agree with the maximum value of our likelihood surface, so we retain the best fit identified using the method of Reino et al. (2021).

The equations from Yang et al. (2020) used to calculate the likelihood are given in Equations (6) and (7). Here  $D$  is the distance between particles in action space normalized by the standard deviations of all the actions.  $\mathcal{P}(\ln D)$  is a probability distribution describing the distance between stars in action space, which is computed using Equation (6) and the two-point correlation function. We set a maximum value of  $D_{\text{max}}$ , as at large distances the behavior will change due to an insufficient number of pairs.

$$1 + \xi \ln D = \frac{D_{\text{max}} \mathcal{P}(\ln D)}{3D^3 \int_{-\infty}^{\ln D_{\text{max}}} \mathcal{P}(\ln D') d \ln D'} \quad (6)$$

$$\ln(\mathcal{L}) = N_{\text{pairs}} \int_{-\infty}^{\ln D_{\text{max}}} \mathcal{P}(\ln D) \ln[1 + \xi(\ln D)] d \ln D. \quad (7)$$

## 3. Data Selection

We have considered five different tidal streams—GD1, Orphan, Palomar 5, Nyx (Necib et al. 2020), and the Helmi stream (Helmi et al. 1999). We find that for some potentials the Helmi stream produces large uncertainties, and is not included in our primary results. Recent work finds that the Helmi stream provides a constraint for the shape of the inner dark matter halo of the MW (Dodd et al. 2022), noting that this stream may be in





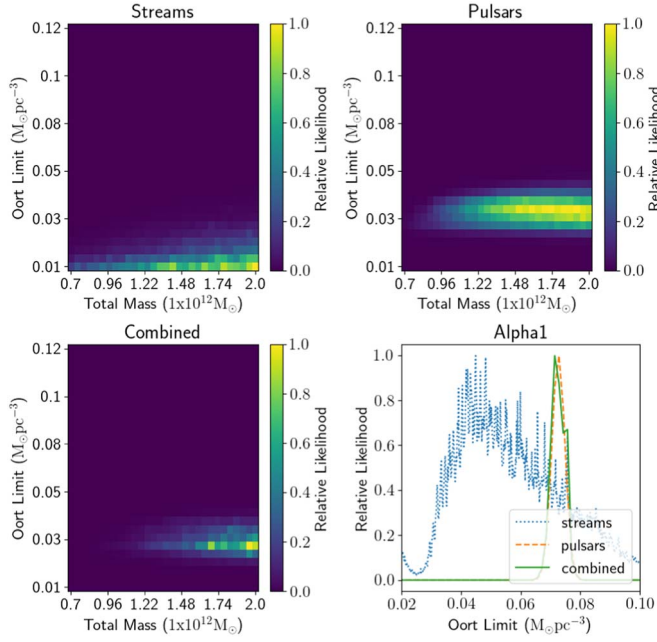


**Figure 3.** Likelihood surfaces for the two-component Staeckel and  $\alpha_1$  potentials. Included are the stream, pulsar, and combined relative likelihood surfaces in both potentials. In this case we can see the general trends in the Oort limit that appear across all of our models, where the streams have a lower value for the Oort limit along with higher uncertainties.

**Table 1**  
Best-fit Parameters and KLD Values

Potential	KLD	Best-fit Parameters	$\rho_{\text{local}} (M_{\odot} / \text{pc}^3)$
Hernquist	0.95	$M = 7.0 \times 10^{11} M_{\odot}$ $a = 8.66 \text{ kpc}$	$0.021 \pm 0.02$
$\alpha\gamma$	0.22	$\log_{10}(\alpha_1/\text{Gyr}^{-2}) = 3.32$ $\log_{10}(\gamma/\text{Gyr}^{-2}) = -5.52$	$0.037 \pm 0.023$
$\alpha\beta$	0.221	$\log_{10}(\alpha_1/\text{Gyr}^{-2}) = 3.31$ $\beta = -0.16$	$0.036 \pm 0.03$
$\alpha_1$	0.224	$\log_{10}(\alpha_1/\text{Gyr}^{-2}) = 3.36$	$0.045 \pm 0.015$
Isochrone	1.07	$M = 1.55 \times 10^{12} M_{\odot}$ $b = 11.92 \text{ kpc}$	$0.029 \pm 0.02$
Two-component Staeckel	1.32	$M_t = 2.23 \times 10^{12} M_{\odot}$ $k = 0.33$ $a_{\text{inner}} = 18.00 \text{ kpc}$ $a_{\text{outer}} = 37.78 \text{ kpc}$ $e_{\text{inner}} = 1.95$	$0.026 \pm 0.02$
MWPotential2014	0.53	Bovy (2015) Values	0.101
Best-fit Pulsars	...	$\log_{10}(\alpha_1/\text{Gyr}^{-2}) = 3.61$	$0.08^{+0.05}_{-0.02}$

**Note.** The KLD optimization results are for a number of different potentials from the GD1, Palomar 5, and Orphan streams. The two-component Staeckel model provides most clustered actions with a KLD of 1.51. Most of these results lack the Nyx stream in order to minimize potential contamination. The two-component Staeckel model includes this data set, however, as it is our best-fit stream result without the Nyx stream, and the results are only slightly altered as a result of the inclusion of this data set. This allows for potential constraints with phase-space overlap with the pulsar sample.

primarily constrain the acceleration in the vertical direction, so we compare the accelerations from the two methods in the vertical direction. We can write the difference in the accelerations as the function specified in Equation (8). A plot of the vertical accelerations of our preferred models can be seen in Figure 4,

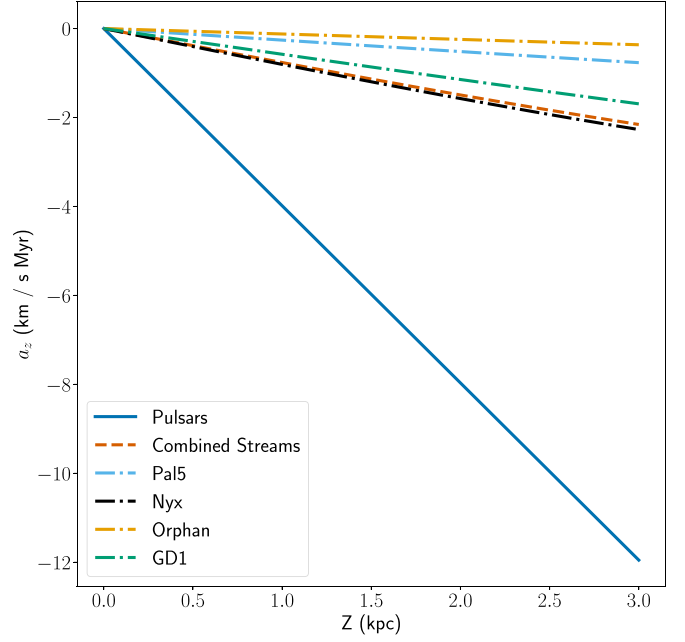


**Figure 4.** Vertical accelerations for the pulsars and the streams. The pulsars are shown in their best-fitting  $\alpha_1$  potential, while the streams are shown in their best-fitting two-component Staeckel potential. We show the sample with the combined stream data set as well as each stream individually.

where  $\alpha_{1,\text{pulsar}} = 4073^{+1422}_{-837} \text{ Gyr}^{-2}$  is the value of  $\alpha_1$  that is derived from the measured pulsar accelerations and  $\Phi$  is the best-fit potential for the streams. Consistent with the lower Oort limit values, the stream samples yield smaller vertical accelerations.

$$f(z) = \alpha_{1,\text{pulsar}} z - \frac{\partial \Phi}{\partial z}. \quad (8)$$

## 5. Conclusions




1. We analyse clustering in action space to determine the best-fit potential for a set of stellar streams that have also been analysed by Reino et al. (2021), with the addition of the Nyx stream. We compare the derived fundamental parameters that describe our galaxy from stellar streams to recent direct acceleration measurements from pulsar timing (Chakrabarti et al. 2021a).
2. We consider several potential models, including Hernquist potentials, isochrone potentials, Staeckel potentials, and the potentials used in analysing the pulsar sample. We analyse Staeckel potentials with both one and two components. The preferred potential for the streams is the two-component Staeckel model, which is the same model considered in Reino et al. (2021) and produces the most clustered actions for our streams.
3. We focus primarily here on the mass of the galaxy and the Oort limit, where the streams provide stronger constraints on the mass and the pulsars provide optimal constraints on the Oort limit. We find that the best-fit potentials for the stellar streams underestimate the Oort limit compared to the value derived from the measured accelerations from pulsar timing. For the potential masses in the two-component Staeckel model, we obtain  $M_{\text{streams}} = 2.23 \pm 0.75 \times 10^{12} M_{\odot}$ ,  $M_{\text{pulsars}} = 1.95 \pm 1.3 \times 10^{12} M_{\odot}$ , and  $M_{\text{combined}} = 1.98 \pm 0.65 \times 10^{12} M_{\odot}$ . Our estimated Oort limits in this potential

are  $\rho_{\text{streams}} = 0.026 \pm 0.02 M_{\odot} \text{pc}^{-3}$  and  $\rho_{\text{pulsars}} = 0.036 \pm 0.011 M_{\odot} \text{pc}^{-3}$ . These values can be compared to the Oort limit of the pulsar's preferred potential determined from direct acceleration measurements, which is  $0.08^{+0.05}_{-0.02} M_{\odot} \text{pc}^{-3}$ . The pulsar sample provides better constraints since these local accelerations are highly dependent on the local density, which drives the vertical component of the acceleration.

4. The Oort limit obtained from the joint constraints of streams and pulsars is lower than the Oort limit derived from pulsars alone, with a value of  $0.031 \pm 0.01 M_{\odot} \text{pc}^{-3}$ . However, pulsars alone do not currently constrain the mass of the potential, since the pulsars are distributed within  $\sim 1$  kpc of the Sun.
5. We provide a fitting formula that may be used to calibrate vertical accelerations of stellar streams to the measured pulsar accelerations.

We thank the referee for useful comments that allowed us to improve this paper. We are grateful to Stella Reino for sharing her scripts for calculating KLD values. S.C. and R.E.S. gratefully acknowledge support from NSF grant AST-2007232. S.C. also acknowledges support from RCSA's Scialog Time Domain Astrophysics Program. R.E.S. acknowledges support from NASA grant 19-ATP19-0068, from the Research Corporation through the Scialog Fellows program on Time Domain Astronomy, and from HST-AR-15809 from the Space Telescope Science Institute (STScI), which is operated by AURA, Inc., under NASA contract NAS5-26555. This work has made use of data from the European Space Agency (ESA) mission Gaia (<https://www.cosmos.esa.int/gaia>), processed by the Gaia Data Processing and Analysis Consortium (DPAC, <https://www.cosmos.esa.int/web/gaia/dpac/consortium>). Funding for the DPAC has been provided by national institutions, in particular the institutions participating in the Gaia Multilateral Agreement.

### ORCID iDs

Peter Craig  <https://orcid.org/0000-0002-3673-0668>  
 Sukanya Chakrabarti  <https://orcid.org/0000-0001-6711-8140>  
 Robyn E. Sanderson  <https://orcid.org/0000-0003-3939-3297>

### References

Banik, N., & Bovy, J. 2019, *MNRAS*, **484**, 2009  
 Batsleer, P., & Dejonghe, H. 1994, *A&A*, **287**, 43  
 Binney, J., & Tremaine, S. 2008, *Galactic Dynamics* (2nd edn.; Princeton, NJ: Princeton Univ. Press), doi:[10.1515/9781400828722](https://doi.org/10.1515/9781400828722)

Bonaca, A., Geha, M., Küpper, A. H. W., et al. 2014, *ApJ*, **795**, 94  
 Bonaca, A., & Hogg, D. W. 2018, *ApJ*, **867**, 101  
 Bonaca, A., Hogg, D. W., Price-Whelan, A. M., & Conroy, C. 2019, *ApJ*, **880**, 38  
 Bonaca, A., Conroy, C., Hogg, D. W., et al. 2020, *ApJL*, **892**, L37  
 Bovy, J. 2014, *ApJ*, **795**, 95  
 Bovy, J. 2015, *ApJS*, **216**, 29  
 Carlberg, R. G., & Grillmair, C. J. 2013, *ApJ*, **768**, 171  
 Carlberg, R. G., Grillmair, C. J., & Hetherington, N. 2012, *ApJ*, **760**, 75  
 Chakrabarti, S. 2013, *ApJ*, **771**, 98  
 Chakrabarti, S., Bigiel, F., Chang, P., & Blitz, L. 2011, *ApJ*, **743**, 35  
 Chakrabarti, S., & Blitz, L. 2009, *MNRAS*, **399**, L118  
 Chakrabarti, S., & Blitz, L. 2011, *ApJ*, **731**, 40  
 Chakrabarti, S., Chang, P., Lam, M. T., Vigeland, S. J., & Quillen, A. C. 2021a, *ApJL*, **907**, L26  
 Chakrabarti, S., Stevens, D. J., Wright, J., et al. 2022, *ApJL*, **928**, L17  
 Chakrabarti, S., Wright, J., Chang, P., et al. 2020, *ApJL*, **902**, L28  
 Craig, P., Chakrabarti, S., Baum, S., & Lewis, B. T. 2022, *MNRAS*, **517**, 1737–1749  
 Dodd, E., Helmi, A., & Koppelman, H. H. 2022, *A&A*, **659**, A61  
 Erkal, D., Koposov, S. E., & Belokurov, V. 2017, *MNRAS*, **470**, 60  
 Fardal, M. A., Huang, S., & Weinberg, M. D. 2015, *MNRAS*, **452**, 301  
 Gaia Collaboration, Prusti, T., de Bruijne, J. H. J., et al. 2016, *A&A*, **595**, A1  
 Gaia Collaboration, Brown, A. G. A., Vallenari, A., et al. 2018, *A&A*, **616**, A1  
 Helmi, A., White, S. D. M., de Zeeuw, P. T., & Zhao, H. 1999, *Natur*, **402**, 53  
 Johnston, K. V., Zhao, H., Spergel, D. N., & Hernquist, L. 1999, *ApJL*, **512**, L109  
 Koposov, S. E., Rix, H.-W., & Hogg, D. W. 2010, *ApJ*, **712**, 260–273  
 Levine, E. S., Blitz, L., & Heiles, C. 2006, *Sci*, **312**, 1773  
 Malhan, K., & Ibata, R. A. 2019, *MNRAS*, **486**, 2995  
 Necib, L., Ostdiek, B., Lisanti, M., et al. 2020, *NatAs*, **4**, 1078  
 Newberg, H. J., Willett, B. A., Yanny, B., & Xu, Y. 2010, *ApJ*, **711**, 32  
 Newberg, H. J., Yanny, B., Rockosi, C., et al. 2002, *ApJ*, **569**, 245  
 Price-Whelan, A. M., Hogg, D. W., Johnston, K. V., & Hendel, D. 2014, *ApJ*, **794**, 4  
 Price-Whelan, A. M., & Johnston, K. V. 2013, *ApJL*, **778**, L12  
 Quillen, A. C., Pettitt, A. R., Chakrabarti, S., et al. 2020, *MNRAS*, **499**, 5623  
 Reino, S., Rossi, E. M., Sanderson, R. E., et al. 2021, *MNRAS*, **502**, 4170  
 Reino, S., Sanderson, R. E., Panithanpaisal, N., Rossi, E. M., & Kuijken, K. 2022, *MNRAS*, **509**, 5365  
 Sanders, J. L. 2014, *MNRAS*, **443**, 423  
 Sanders, J. L., & Binney, J. 2013, *MNRAS*, **433**, 1813  
 Sanders, J. L., Bovy, J., & Erkal, D. 2016, *MNRAS*, **457**, 3817  
 Sanderson, R. E., Hartke, J., & Helmi, A. 2017, *ApJ*, **836**, 234  
 Sanderson, R. E., Helmi, A., & Hogg, D. W. 2015, *ApJ*, **801**, 98  
 Sharma, S., & Steinmetz, M. 2011, *EnBiD: Fast Multi-dimensional Density Estimation*, Astrophysics Source Code Library, ascl:[1109.012](https://ascl.net/1109.012)  
 Varghese, A., Ibata, R., & Lewis, G. F. 2011, *MNRAS*, **417**, 198  
 Vasiliev, E., Belokurov, V., & Erkal, D. 2021, *MNRAS*, **501**, 2279  
 Virtanen, P., Gommers, R., Oliphant, T. E., et al. 2020, *NatMe*, **17**, 261  
 Wang, S., Necib, L., Ji, A. P., et al. 2022, *arXiv:2210.15013*  
 Weinberg, M. D., & Blitz, L. 2006, *ApJL*, **641**, L33  
 Yang, T., Boruah, S. S., & Afshordi, N. 2020, *MNRAS*, **493**, 3061  
 Zucker, D. B., Simpson, J. D., Martell, S. L., et al. 2021, *ApJL*, **912**, L30